

## The Influence of Filaments on Scrape-Off Layer Transport in MAST

S. Lisgo 1), N. Ben Ayed 2), P. Boerner 3), G. F. Counsell 1), B. Dudson 2), A. Kirk 1),  
D. Reiter 3), S. Tallents 4), and the MAST Team

1) UKAEA Fusion Association, Culham Science Centre, Abingdon, OX14 3DB, UK

2) University of York, Department of Physics, York, YO10 5DD, UK

3) IPP, Forschungszentrum Juelich GmbH, EURATOM, D-52425 Juelich, Germany

4) Imperial College, Prince Consort Road, London, SW7 2BZ, UK

email contact of main author: [steve.lisgo@ukaea.org.uk](mailto:steve.lisgo@ukaea.org.uk)

### Abstract

The tokamak scrape-off-layer (SOL) is a primary component of the interface between the core plasma and the material surfaces of the vacuum vessel. Investigations on the Mega-Ampere Spherical Tokamak (MAST) have been undertaken in an effort to characterise the filamentary nature of the SOL and to assess the influence of this intermittency on traditional steady-state approximations of the plasma transport. Distribution functions for L-mode, ELM and inter-ELM filament properties have been determined from fast camera, reciprocating probe data and time-resolved Thomson scattering measurements, and average values for filament size and motion (including parallel flows within filaments) are reported. A 4D dedicated interpretive code for the boundary plasma is being developed, based on extensions to the OSM-EIRENE package. Initial results for filament evolution are presented, where the filament properties in the simulation are prescribed from the measured data. The model captures the essential features of intermittent transport in the boundary and can therefore be used to quantitatively assess the validity of the steady-state SOL approximation.

### 1. Introduction

An accurate model of SOL processes is required for reliable prediction of the boundary plasma environment in next-step devices such as ITER, in particular the distributions of particle and heat fluxes exhausted to the plasma facing components, and the transport back to the confined plasma of the associated neutral and impurity influxes. In the traditional picture, the SOL is considered to be relatively quiescent (ELMs excepted), with steady-state 2D poloidal profiles resulting from competition between drifts, classical transport parallel to the magnetic field, and “anomalous” transport in the radial direction. However, observations on several devices indicate that plasma intermittency in the SOL is significantly more prevalent than previously thought [1], prompting a re-evaluation of the steady-state approximation and raising the question of whether a new model paradigm must be developed based on transient plasma states, one that explicitly includes filamentary transport. The Mega-Ampere Spherical Tokamak (MAST) is well suited to address this issue due to the combination of high-speed Langmuir probe systems, wide-angle fast camera imaging, and high-performance Thomson scattering systems.

Main chamber camera data have been collected for L- and H-mode (inter-ELM and ELM-resolved), all of which show field-aligned filamentary structures. The toroidal quasi-mode number and the filament dimensions can be determined directly from a single image, while information on filament motion is obtained by mapping of the filament structures to the magnetic reconstruction over several consecutive frames. Outer midplane reciprocating probe data collected using a triple Langmuir probe head have corroborated the observed fluctuations, with  $\delta n / \langle n \rangle$  greater than 1 across the SOL (L-mode) [2]. Parallel flow measurements from a Gundestrup head have provided data for a range of discharge parameters, including values for individual filaments.

Langmuir probe and camera data from the divertor also show intermittency, although at reduced levels near the strike-points. This apparent inconsistency with the high level of plasma fluctuations when mapping to the outer midplane is related to the shear in the pitch angle of the magnetic field near the x-point, which has a smaller scale length than the filaments and therefore acts to toroidally “smear” their radial structure [3]. This suggests that the SOL can be both intermittent and quasi-steady-state at the same time, depending on the relationship of the plasma region in question to the x-point.

A 4D ( $x,y,z,t$  – guiding center only for kinetic components) dedicated interpretive code for the boundary plasma is under development, based on extensions to the OSM-EIRENE package [4,5]. Note that

this is not a first principles predictive code, but rather a semi-empirical model that requires a large amount of experimental information as input, such as data from Langmuir probes, Thomson scattering, spectrometers, cameras (visible and IR), and pressure gauges. Aspects of the plasma solution that are not specified from measurement are largely constrained via conservation equations. The primary objective is to provide the experimentalist with a tool for evaluating SOL transport models in a framework that accurately represents the 3D, time-dependent nature of the problem, facilitating cross-comparisons between otherwise disparate diagnostics and allowing notable deficiencies in the model to guide future experimental investigations. Initial simulation results are presented for filament evolution, including x-point smearing, with filament properties prescribed from measured data. Efforts to provide a physics-based description of filament formation and transport include BOUT++ and ESEL runs [6,7], which will eventually be coupled to the semi-empirical model described here. Processes that vary linearly with density are unlikely to be significantly affected by intermittency, for instance the rate coefficient for  $D_\alpha$  emission has a weak density dependence and time-averaged data have been reproduced to within 30% when assuming steady-state [8]. However, the extent to which the filaments affect non-linear processes is unknown; including impurity production and transport related to intermittent fluxes away from the divertor strike-points, in particular those due to ELMs.

Section 2 describes filament analysis from fast camera imaging, and section 3 presents results from outer midplane Langmuir probe measurements. Section 4 relates the current state of the interpretive model and shows preliminary results.

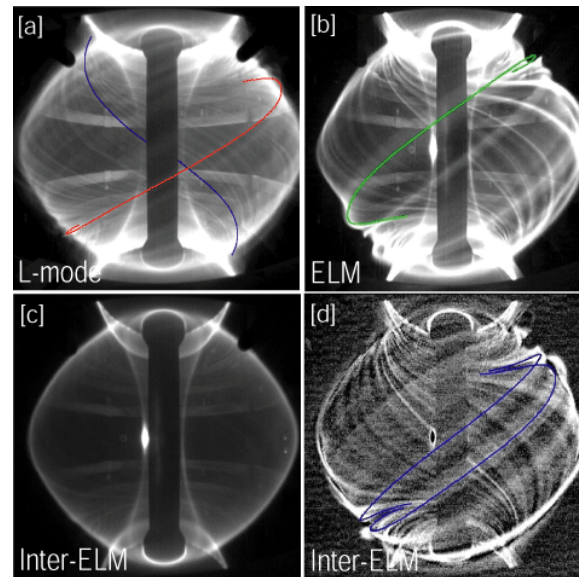


FIG. 1. Filament imaging (unfiltered). (a) L-mode, (b) ELM, (c) inter-ELM, (d) inter-ELM with background subtraction.

## 2. Fast camera analysis of filaments

The geometry of the MAST vessel and, in particular, the large separation between the plasma edge and the vessel wall (typically around 60 cm) makes for excellent visible imaging of edge structures. Combined with a wide-angle lens, this allows views of the entire plasma to be

Parameter	L-mode	Inter-ELM	ELM
$N$ , quasi-toroidal mode number (see text)	20-50	10-40	10-20
$L_{\perp}$ , width in diamagnetic direction (cm)	7-9	9-12	2-6
$L_{rad}$ , width in radial direction (cm)	5-10	3-5	4-6
$V_{\phi}$ , toroidal ( <i>assumed</i> , see text) velocity (km s <sup>-1</sup> )	2-9	3-12.5	10-30
$V_r$ , radial velocity (km s <sup>-1</sup> )	0.5	1-2	1-9
$\tau$ , lifetime ( $\mu$ s)	40-60	50-120	100-180
$n_{e,sep}$ , density when filament at separatrix ( $10^{18}$ m <sup>-3</sup> )	0.6-5	0.5-2	20-60

Table 1: MAST filament parameters for different confinement regimes [6].

taken, an example of which is shown in Figure 1 for all confinement regimes. The camera is a Photron Ultima APX-RS, and is unfiltered so that the observed light is dominated by  $D_{\alpha}$  emission from the electron excitation of the neutral gas surrounding the plasma. Extended filamentary structures can be seen which expand radially far into the SOL and can be tracked up to  $\sim 10$  cm from the last closed flux surface (LCFS). Note that the image in 1(d) has been enhanced by removing the slowly varying background light, leaving only the fast transient features. Filaments are located in space by projecting field lines from EFIT magnetic reconstructions [9,10] onto the images at varying toroidal angle and distance from the LCFS. Using frame rates of 100 kHz, filaments can be tracked over several frames and their toroidal and radial velocities measured. This method has been used to manually measure the properties of L-mode [11], inter-ELM [12, 13] and ELM [14] filaments. These results are summarized in Table 1 for the observed lifetime ( $\tau$ ), radial and toroidal velocities ( $V_r$  and  $V_{\phi}$ ), toroidal mode number  $N$ , radial and perpendicular widths ( $L_{rad}$  and  $L_{\perp}$ ). Several differences between these filaments are apparent, as we now discuss. The lifetime of ELM filaments is found to be longer than those in L-mode and are observed to accelerate radially outwards from the plasma edge (as indicated by the range in  $V_r$  in table 1) [14]. L-mode and inter-ELM filaments do not appear to accelerate in the SOL.

Toroidal rotation of filaments is always observed to be in the co-current (ion diamagnetic drift) direction in all regimes. Note that it is not possible from these images to distinguish between toroidal and poloidal rotation and so here all perpendicular velocities are quoted as purely toroidal. Rotation speeds for L-mode filaments are typically 3–4 km s<sup>-1</sup>, though filaments are observed with a wider spread as shown in Table 1. For L-mode, this rotation is found to be approximately constant for any given filament, but to vary between filaments. This results in constantly changing spacing of filaments, complicating the definition of mode number. Hence the mode numbers  $N$  listed in Table 1 are pseudo-mode numbers which estimate the number of filaments in 360°. This rotation also produces blurring of the filaments over the 10  $\mu$ s integration time, which has been taken into account.

In H-mode, the edge plasma tends to rotate faster and indeed ELM filaments are observed to rotate faster than those in L-mode. Inter-ELM filaments, however, do not rotate much faster than L-mode filaments: two possible explanations for this are that inter-ELM filaments originate closer to the plasma edge (where the bulk plasma rotation is slower) than ELMs or

that inter-ELM filaments rotate at a different rate relative to the bulk plasma than ELMs. Either of these would indicate different driving processes. Distinguishing between driving processes is difficult with only typical values. An effort to quantify transport dependencies on bulk plasma parameters for inter-ELM filaments is presented in the next section.

## 2.1 Focus on inter-ELM filaments

Whilst previous efforts have been dedicated to the study of fluctuations in L-mode [14,15,16] and ELMy H-mode [17,18,15] phases, few efforts have concentrated on the inter-ELM phase, i.e. the period between ELMs, as shown in Figure 1 (c) and (d). As a result, our understanding of edge transport phenomena during these periods is still limited. Transport in the SOL of inter-ELM periods in the NSTX device has been shown to

include blob-like structures in the radial vs poloidal plane using the gas puff imaging (GPI) diagnostic [19]. More recently, large scale fluctuations, thought to be due to 3D helical structures, have been found in ASDEX Upgrade during inter-ELM periods using both the vertical Thomson scattering system and electron cyclotron emission (ECE) diagnostics [20]. In this section, analysis of the filamentary nature of the transport during H-mode inter-ELM periods in the MAST is presented.

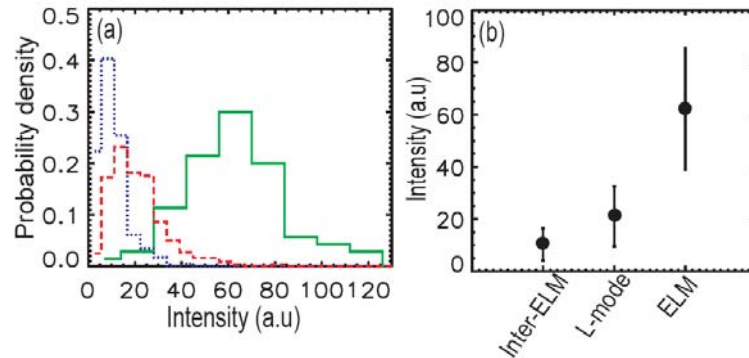


FIG. 2. PDFs of light intensity corresponding to L-mode (dashed-red), inter-ELM (dotted-blue) and ELM (solid-green) filaments, for the same discharge. The mean intensity of each distribution and the RMS are plotted in (b). Light intensity of fluctuations in the SOL vary considerably: inter-ELM filaments are the lowest-level fluctuations, followed closely by the L-mode phase, whilst ELM filaments dominate the light emission.

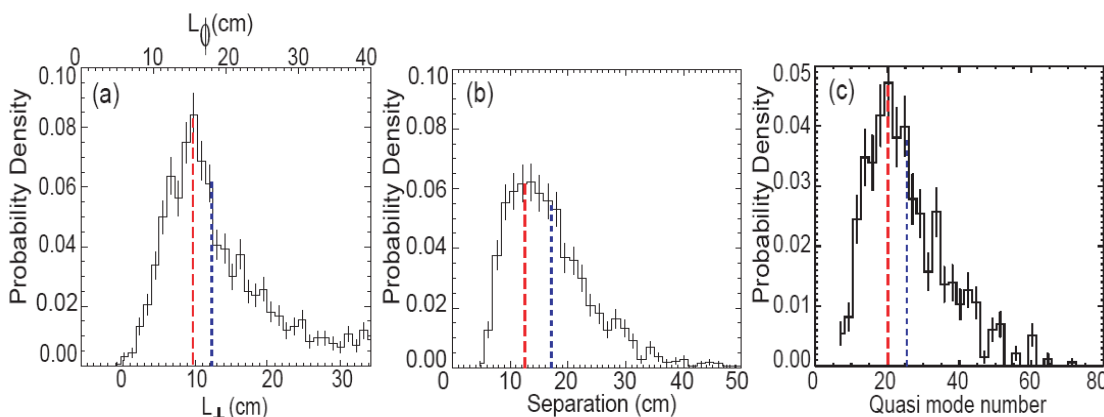


FIG. 3. Probability density functions (PDF's) of (a) filament perpendicular widths ( $L_{\perp}$ ); the top x-axis corresponds to the original measured widths ( $L_{\phi}$ ), (b) separation between filaments ( $\Delta r$ ) and (c) the number of filaments per toroidal circuit ( $N$ , quasi mode-number). Peak and mean values are marked by long and short dashed lines respectively.

Similar to L-mode and ELM filaments, inter-ELM filaments are seen to be aligned with the local magnetic field [14]. The magnitudes of the relative light intensity fluctuations across the discharge vary considerably in the SOL, with maximum registered relative amplitudes of 14, 40 and 140 in arbitrary units for inter-ELM, L-mode and ELM regimes respectively. Automated analysis of high-speed camera images has afforded an important advance: the production of probability distribution functions (PDF's) in order to gain a more complete picture of filament behaviour. Specifically, the distributions are critical to increasing the accuracy of the interpretive transport model (Section 4). The inter-ELM PDF for  $D\alpha$  emission at the outer midplane is shown in Figure 2, along with data for L-Mode and ELMy H-mode.

Examination of 2000 filament widths ( $L_{\perp}$ ) in MAST beam-heated discharge #15622 ( $I_p \sim 0.73$  MA,  $B_0 \sim 0.51$  T;  $n_{GW} \sim 0.3-0.5$ ;  $q_{95} \sim 5-6.5$ ) reveals a non-Gaussian probability distribution, shown in Figure 3(a), with a peak value (most likely) of  $\sim 10$  cm, and a mean value of  $\sim 11.5$  cm. The long tails are mainly due to (a) the occurrence of closely-spaced and overlapping filaments whose separate widths have been measured as single filament widths, and/or (b) enhanced blurring resulting from filament rotation above 9 km/s. In addition to filament widths, a survey of the separation ( $\Delta r$ ) between filaments has also been measured: The PDF, shown in Figure 3 (b), leads to a peak value (most likely value) for filament separation of  $\Delta r \sim 15$  cm and a mean value of  $\sim 18$  cm. The peak separation has also been used to infer a peak quasi toroidal mode number  $N \sim 24$  using the expression  $N = 360^\circ / \Delta r$ . Toroidal mode numbers have also been calculated directly from the number of observed filaments which span the full toroidal circuit on the full view images. Mode numbers within the same discharge are found to vary significantly: they are found to be in the range 10–40 with a peak value of 20 and a mean,  $N_{\text{inter-ELM}} \sim 26$ . This range is in good agreement with the observed mode number range on ASDEX Upgrade using the vertical Thomson scattering system [21].

In order to investigate any dependence of filament motion on plasma parameters, toroidal and radial displacements of filaments have been tracked over a wide variety of parameters

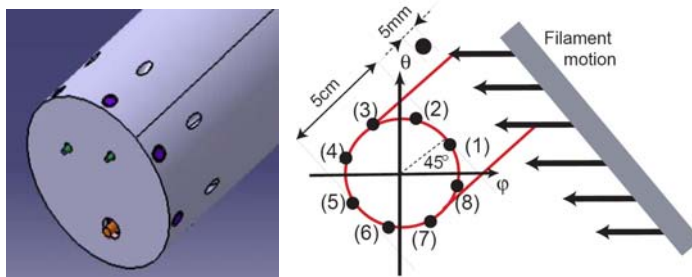


FIG. 5. Outer midplane reciprocating probe “Gundestrup” head, with 8 tips located at the end of the probe (purple).

mean radial velocities are  $\sim 1.45$  km/s and 1.2 km/s, respectively, for high and low densities

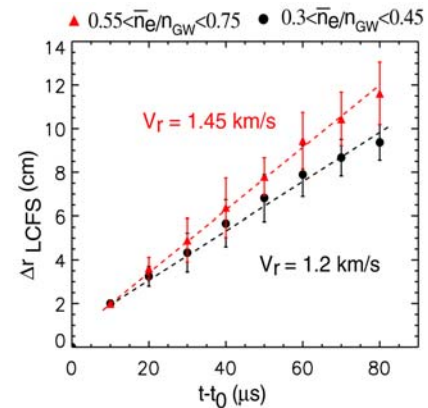


FIG. 4. Radial velocities of inter-ELM filaments as a function of core line-averaged density.

involving the line-averaged density, toroidal field, plasma current, and neutral beam heating power. Whilst no significant changes are observed with  $B_\phi$ ,  $I_p$  and  $P_{\text{NBI}}$ , motion of these filaments has been found to have a strong dependence on  $\langle n_e \rangle$ . Figure 4 shows the radial velocity of inter-ELM filaments, where the

### 3. Parallel flows in filaments

The outboard midplane reciprocating probe (RP) system on MAST is equipped with a circular array of 8 equally spaced, flush-mounted Langmuir probes arranged in diametrically opposite pairs; see Figure 5. These probes are biased to  $-200\text{V}$ , and used to measure the ion saturation current,  $I_{\text{sat}}$ .

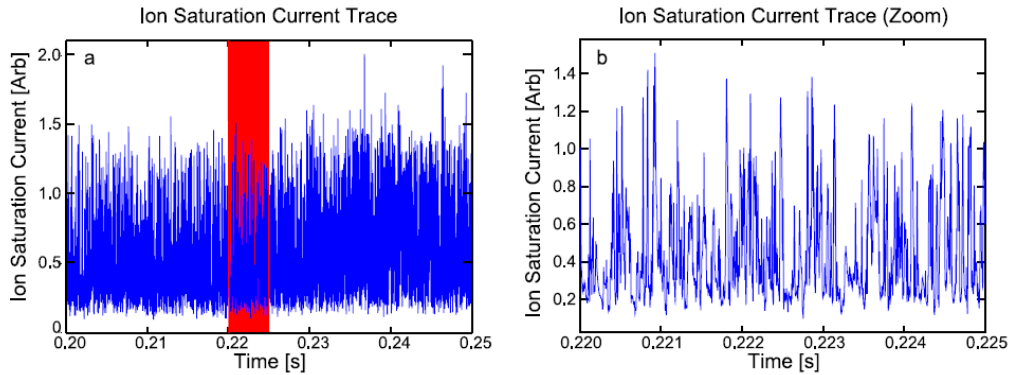


FIG. 6. Typical saturation current data from the Gundestrup probe, sampled at 500 kHz. The right hand pane is an expanded plot of the red highlighted region on the left.

The data are highly intermittent, as illustrated in Figure 6. The distributions of ion saturation currents are formulated using advanced methods: an ‘‘Adaptive Kernel Estimate’’ [22] is used to generate an optimally smoothed histogram in both the peak and tail of the distribution, unbiased by binning choices, and a Monte-Carlo re-sampling technique known as the ‘‘Bootstrap Method’’ [23] is applied to estimate the uncertainties of the distribution function and its moments. Assuming the distribution of the ion-saturation current density on all pins should be the same in the absence of flows, by comparing normalised bin numbers (high and low percentiles) from the distribution of current on each pin using the standard interpretations for Gundestrup Probes, the parallel flow in the filament and the ambient plasma may be resolved independently.

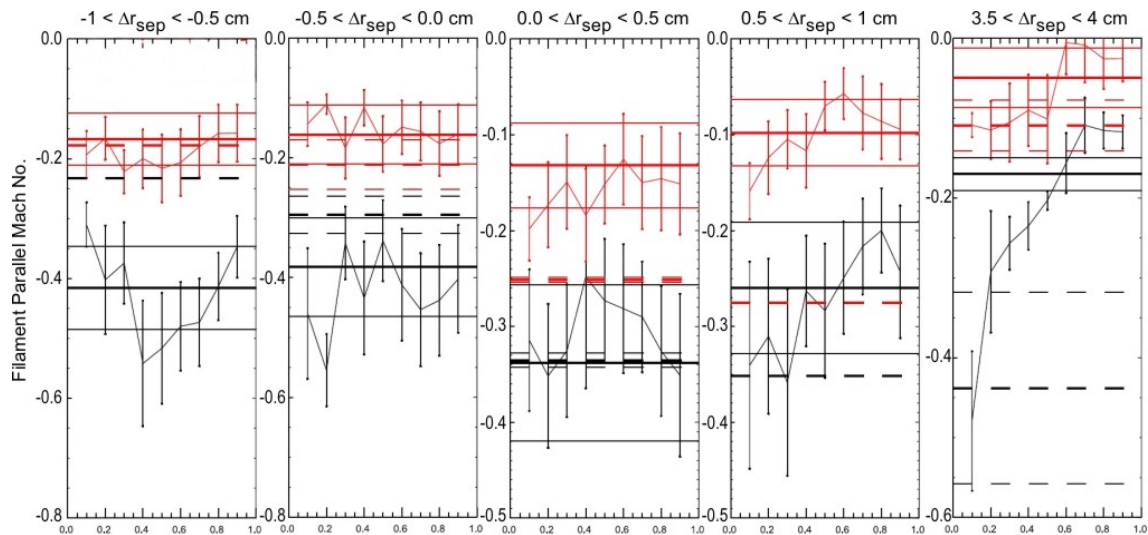


FIG. 7. Calculated parallel Mach numbers in filaments for a range of distances to the separatrix at the outer midplane,  $\Delta r_{\text{sep}}$ . The independent axis is the normalised bin number across the PDF of the ion saturation current. The black traces are Mach numbers from magnetised probe theory (ion gyroradius smaller than the pin area), and the red traces from unmagnetised theory. The horizontal solid lines are the flow calculated from mean  $i_{\text{sat}}$  and the dashed are from the most frequent  $i_{\text{sat}}$ .

Data is presented for a range of probe positions relative to the separatrix in Figure 7. Traces from both magnetised [24] and un-magnetised [25] probe theory are presented since the gyroradii of ions along the probe trajectory are on the order of the Langmuir probe pin collection areas. The average Mach numbers are between 0.2 and 0.4 near the separatrix, decreasing to with distance outboard of the separatrix. Detailed analysis is ongoing.

#### 4. Interpretive filament modelling

The experimental data on the size, motion and plasma conditions (the latter are from Thomson scattering data acquired in “burst mode”, not shown here) of MAST filaments are used as input to an empirical model of intermittent structures and transport in the scrape-off layer. A 3D version of the OSM-EIRENE code package has been developed, where OSM generates the modelling grid and formulates a fluid description of the SOL, and the EIRENE Monte-Carlo kinetic transport code follows neutral particles and impurity ions. The computational domain, which generally includes the entire vacuum vessel volume, is divided into tetrahedrons. A filament cross-section is defined at the midplane, based on the measured filament size parameters (Table 1), and traced to the target plates with the assumption that the plasma structure is aligned with the magnetic field. The tetrahedron mesh is then locally refined along these field line trajectories. The codes iterate, with the field line bundle moving toroidally and radially as per the measured velocities. This setup provides a geometric framework for interpolating filament models onto the refined regions of the tetrahedron grid, i.e. the regions in the 3D mesh that are spatially well resolved. In future, source and motion data from turbulence codes, such as ESEL or BOUT++, could also be employed, rather than experimental data.

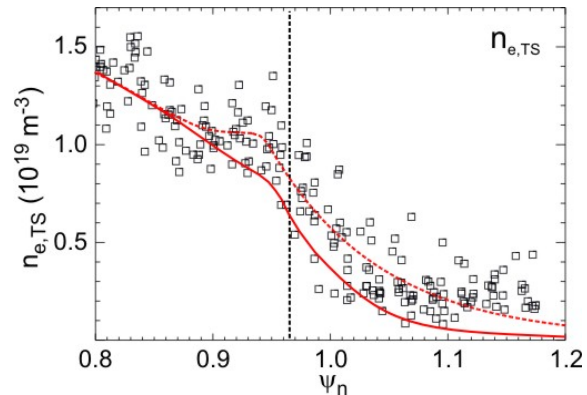


FIG. 8. Upstream Thomson scattering data for L-mode MAST discharge 15169. The dotted line is the best fit. The solid line is the assumed “background”, or diffusive plasma, in the absence of filaments.

Upstream Thomson scattering data from Ohmic discharge 15169 at 259 ms are plotted in Figure 8. In the initial implementation of the simulation, filaments are transported “on top of” a background hydrogenic plasma, i.e. an approximate representation of the ambient plasma that would be present in the SOL even in the absence of filaments (which, interestingly, is similar to an inter-ELM H-mode SOL plasma [2]). This is taken to be the lower fit to the data shown in the figure, with the same reasoning applied to the target Langmuir probe data (not shown).

Figure 9 shows an example of filament  $D_\alpha$  light in the main chamber, where the  $D_\alpha$  emission from the background plasma has been subtracted. The structures are field-aligned, but only have a quasi-mode number of 12, which is the (temporary) limitation of the simulation hardware. The left-hand edge of the centre-column is outlined in green. Integration of the calculated emission over multiple time-steps allows a direct comparison between long integration time diagnostics and transport models applied to filament evolution. Impurity tracking modules currently in development for EIRENE will be used to address erosion and mass transport dynamics related to filament interaction with the wall.

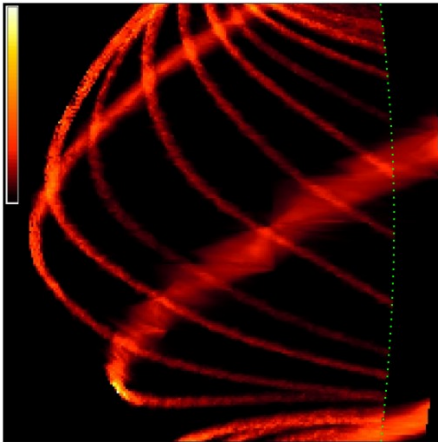


FIG. 9. Simulated  $D_\alpha$  filtered camera image from the main plasma in MAST (discharge 15169) from the OSM-EIRENE code. The background  $D_\alpha$  light has been subtracted in order to highlight the filaments.

## 5. Summary

A combination of fast camera imaging and midplane reciprocating probe measurements have been used to characterise filamentary transport in the SOL of the MAST tokamak, for a range of core plasma confinement regimes (L-mode, ELMy H-mode, and inter-ELM H-mode). The toroidal and radial velocities, the size of the filaments, and their plasma content have been inferred, with several of the quantities expressed as probability distribution functions. These filament properties have subsequently been used to constrain the transport model for filaments in the OSM-EIRENE code, which has been extended to include a generalised 3D representation filament structure and their evolution in time. Efforts are now underway to refine the model and simulate the effect of filaments on target plate and first wall structures.

This work was jointly funded by the United Kingdom and Physical Sciences Research Council and by the European Communities under the contract of the Association between EURATOM and UKAEA. The views and opinions expressed herein do not necessarily reflect those of the EC.

- [1] S. J. Zweben, *et al.*, Plasma Phys. Control. Fusion **49** (2007) S1–S23
- [2] G. F. Counsell, *et al.* IAEA Proceedings, Chengdu (2006).
- [3] A. Kirk, *et al.*, Plasma Phys. Control. Fusion **49** (2007) 1259–1275
- [4] S. Lisgo, *et al.*, J. Nucl. Mater. **337-339** (2005) 256
- [5] Reiter D, *The EIRENE Code*, <http://www.eirene.de>
- [6] B. D. Dudson, *et al.*, Plasma Phys. Control. Fusion, *submitted to journal*
- [7] S. Tallents, Ph.D. Thesis, *in preparation*
- [8] S. Lisgo, *et al.*, EPS Conference, 2007
- [9] EFIT Equilibrium Code at Culham. <http://fusion.org.uk/EFIT/>
- [10] Lao L L, St John H, Stambaugh R D, Kellman A G and Pfeiffer W 1985 *Nucl. Fusion* **25** 1611–22
- [11] Dudson B D 2008 Edge turbulence in the Mega-Amp Spherical Tokamak *PhD Thesis* University of Oxford
- [12] Ben Ayed N, Kirk A, Dudson B, Tallents S, Vann R G L, Wilson H R and the MAST team 2008 Characterising AQ6 edge turbulence in inter-ELM periods in the MAST tokamak *Plasma Phys. Control. Fusion* *submitted*
- [13] Ben Ayed N, Kirk A, Dudson B, Vann R G L, Tallents S, Wilson H R and the MAST Team 2008 *35th EPS AQ7 Plasma Physics Conf.*
- [14] Kirk A *et al* 2006 *Plasma Phys. Control. Fusion* **48** B433–41
- [15] Dudson B D *et al* 2005 Plasma Phys. Control. Fusion **47** 885-901.
- [16] Counsell G F *et al* 2006 In 21st Fusion Energy Conference, Chengdu, China, IAEA
- [17] Kirk A *et al* 2004 Phys. Rev. Lett. **92** 245002
- [18] Kirk A *et al* 2004 Plasma Phys. Control. Fusion **46** 551-572
- [19] Kirk A *et al* 2005 Plasma Phys. Control. Fusion **47** 315-333
- [20] Zweben S J *et al* 2004 Nucl. Fusion **44** 134
- [21] Kurzan B *et al* 2007 Plasma Phys. Control. Fusion **49** 825-844
- [22] L. Brieman, W. Meisel and E. Purcell, *Technometrics* **19** (1977), 135-144
- [23] B. Efron, *The Annals of Statistics* **7** (1979) 1-26
- [24] I. H. Hutchinson, *Phys. Fluids* **30** (1987) 3777-3781; J. P. Gunn, *et al.*, *Phys. of Plasmas* **8** (2001) 1995-2001
- [25] I. H. Hutchinson, Plasma Phys. Control. Fusion **44** (2002) 1953-1977; S. Kado, *et al.*, *Phys. of Plasmas* **12** (2005), 044504